Chapter 18
FEM Human Body Model with Embedded Respiratory Cycles for Antenna and E&M Simulations

Anh Le Tran, Gregory Noetscher, Sara Louie, Alexander Prokop, Ara Nazarian, and Sergey Makarov

18.1 Background

Human respiration is the exchange of air between the lungs and the ambient atmosphere. Below, we briefly summarize some major facts pertinent to our study.

Mechanics. Respiratory mechanics represent a complex multi-object deformation process. It predominantly involves the non-rigid motion of the (i) diaphragm; (ii) thoracic cage including ribs, cartilage, and sternum; (iii) lungs; (iv) heart; (v) liver; (vi) kidneys; and (vii) intestine. For inhalation, the diaphragm contracts and pushes the contents of the abdomen in the inferior direction as shown in Figs. 18.1 [1] and 18.2 [2]. Simultaneously, the external intercostal muscles expand the rib cage and slightly raise it. For exhalation, the diaphragm and the external intercostal muscles relax.

A. Le Tran
ECE Department, Worcester Polytechnic Institute, Worcester, MA, USA

G. Noetscher (✉)
Worcester Polytechnic Institute, Worcester, MA, USA
e-mail: gregn@wpi.edu

S. Louie
ANSYS, Inc., Canonsburg, PA, USA

A. Prokop
CST-Computer Simulation Technology AG, Darmstadt, Germany

A. Nazarian
Center for Advanced Orthopaedic Studies at Beth Israel Deaconess Medical Center, Harvard Medicine School, Boston, MA, USA

S. Makarov
Massachusetts General Hospital, Boston, MA, USA

Worcester Polytechnic Institute, Worcester, MA, USA

S. Makarov et al. (eds.), *Brain and Human Body Modeling*,
https://doi.org/10.1007/978-3-030-21293-3_18

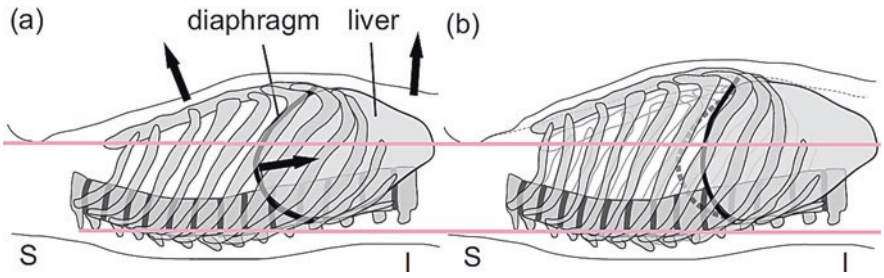

Fig. 18.1 (**a**) Maximum exhalation position, (**b**) maximum inhalation position, after [1]

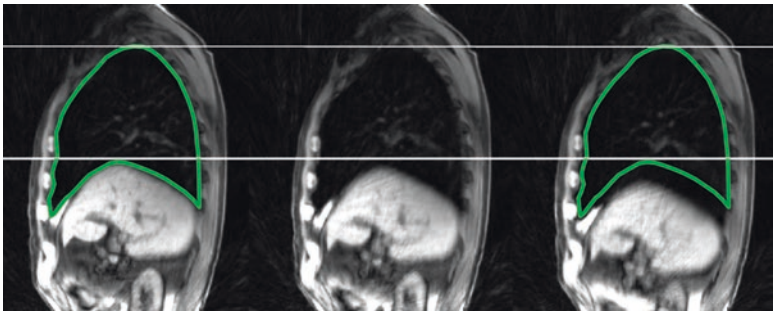

Fig. 18.2 Respiratory motion captured via MRI retrospective gating and averaging over multiple cycles, after [2]. The green contour indicates lung volume at maximum exhalation

Diaphragm motion. Respiration is chiefly driven by the diaphragm with primary motion in the superior-inferior direction; total travel is estimated as 10–30 mm during quiet breathing [1]. Other studies report 20 ± 7.0 mm average [2]. A simplified 1D diaphragm motion, $x(t)$, is non-harmonic, and the exhalation portion dominates the inhalation. Given the exhalation at origin, one has

$$x(t) = -A\cos^4 \omega t \tag{18.1}$$

where A is the corresponding amplitude [3, 4]. Furthermore, the respiratory motion often exhibits hysteresis in space, with an amplitude on the order of 2–4 mm [1].

Adjacent tissues. Closely adjacent structures (i.e., liver, etc.) show comparable motion amplitudes. Furthermore, the following motion amplitudes have been observed (cf. a review in Ref. [1]):

- Motion with an average amplitude of 12 mm in the lung for targets not attached to rigid structures
- 1–25 mm superior-inferior motion of the kidneys, 13 mm superior-inferior motion of the spleen, 2–8 mm motion of the heart (the heart motion is mostly a simple rigid-body translation [5, 6]), and 1–7 mm motion of the trachea
- 13 mm superior-inferior motion of the spleen

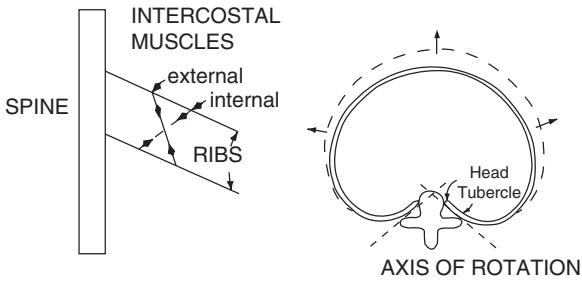

Fig. 18.3 Motion of the ribs during respiration, after [5, 7]. The ribs rotate about an axis through their costal neck

Thoracic cage kinematics. During respiration, the ribs rotate about an axis through their costal necks to affect the anteroposterior and transverse diameters of the thoracic cavity as shown in Fig. 18.3 [5, 7].

CAD B-Spline modeling. Modeling of the breathing cycle to date has been mostly performed via deformable NURBS surfaces (B-splines) for the lungs and surrounding tissues. The changes the phantoms undergo are then typically splined over time to create time continuous 4D respiratory models [5, 8, 9], which indeed utilize free-form deformations.

Challenges of FEM CAD Modeling. Commercial FEM codes do not operate with B-spline surfaces but rather with triangulated surfaces and tetrahedral/hexahedral volumes. This is in particular valid for most frequency-domain electromagnetics solvers such as ANSYS EM Suite/Maxell 3D and CST Microwave Studio. Therefore, a free-form breathing sequence has to be ultimately converted to a (large) discrete series of separate (full-body) triangulated CAD models, even if the original data were in the form of parametric B-splines. Generally, a conversion from NURBS surfaces to FEM triangular surfaces requires very significant additional meshing times.

The size of one detailed FEM full-body model is quite large (about 200–1000 Mbytes in ANSYS) and a computation with 20–30 such models would be a significant challenge from several points of view. For example, a user will need to create, run, and then post-process a number of large distinct project files, each of which must replicate his/her own excitation setup (e.g., a coil, an antenna, or a radar) and employ a new human model. Furthermore, manual repositioning is necessary for any and all on-body and in-body devices at every step, which would potentially create errors.

18.2 Methods

Built-in affine transformations. A commercial CEM package typically includes a set of nine affine transformations:

Three translations (in the x, y, z directions)
Three rotations (about the x, y, z axes)
Three directional scaling transformations (along the x, y, z axes)

applicable to any object (including a triangular tissue mesh) or to a group of objects and in the form of a parametric sweep. These transformations can be performed in

either global or local coordinate systems. The user can initialize a discrete generic global variable, x_n, $n = 0,\ldots,N$, define object geometry parameters as certain unique functions of x_n, and then move, rotate, or deform every object of a multi-object structure independently within the framework of the same project file.

Our approach. We apply built-in parameterized affine transformations to construct breathing cycles (quiet, deep, shallow) using only one base full-body human model [10] source not found and using only one project file. Along with the base static human CAD model, this project file includes a parametric sweep or sweeps modeling deformations of involved tissues. Such an approach is not exact, but it may have sufficient accuracy when the parametric sweep is carefully designed. It will allow us to employ any temporal resolution, which is impossible with discrete models. To construct an anatomically relevant breathing cycle, we will try to follow the anatomical data collected from Refs. [1–9] as close as possible.

Challenges. To design an FEM-compatible and anatomically justified multi-tissue affine parametric sweep, a very extensive preprocessing of the static human CAD model is necessary, which is a significant undertaking.

18.2.1 Selecting a Sweeping Variable

The natural sweeping variable x_n is proportional to *the diaphragm motion*. Since the breathing cycle is periodic, only one period T must be considered. According to Eq. (18.1), physical time, t, is expressed through a sweep variable by

$$t = T\left\{\frac{1}{2} - \frac{1}{\pi}a\cos\left(\sqrt[4]{\frac{x_n}{N}}\right)\right\} \text{ when } 0 \le t \le T/2 \tag{18.2}$$

This result can be programmed in MATLAB as

E = 11; t_=0:E; T = 1; t = T∗(pi/2-acos((t_/E).^0.25))/pi; plot(t_, t, '-∗'); grid on.

Table 18.1 gives the corresponding numerical time values. Sweeping variable x_n runs from zero to $N = 11$ in 12 uniform steps. Its zero value corresponds to maximum exhalation; its maximum value of 11 corresponds to maximum inhalation. Higher N values can be considered for a better accuracy.

18.2.2 Static CAD Model

As a base human model at maximum exhalation, we will choose the VHP-Female v.3.1 CAD model (http://www.nevaem.com/) shown in Fig. 18.4. The source data for this model was provided by the National Library of Medicine's Visible Human Project in the form of full color cryosection images. These images were hand segmented and registered in a global coordinate frame. The model has 26 individual tissues, 270 individual tissue parts, major blood vessels and peripheral nerves, and

Table 18.1 Time values in terms of period, T, corresponding to the sweeping variable x_n, $n = 0, \ldots, N$ for $N = 11$

x_n	t/T
0	0.0000
1	0.1850
2	0.2265
3	0.2571
4	0.2830
5	0.3066
6	0.3292
7	0.3515
8	0.3747
9	0.4000
10	0.4308
11	0.5000
10	0.5692
9	0.6000
8	0.6253
7	0.6484
6	0.6708
5	0.6934
4	0.7170
3	0.7429
2	0.7735
1	0.8150
0	1.0000

a superior resolution in the spinal cord/cranium. All tissue structures are manifold shells and no shell intersects with any neighboring shell. The sweep for the respiratory motion will be implemented for both BASE and SMOOTH sub-models. Only the results for the BASE sub-model will be reported here.

The subject is a ~60-year-old white female with a height h of 162 cm measured from top of the scalp to the average center of both heels. The body mass M, computed using standard tissue densities [11] and assigning the average body shell, which includes internal tissues, the density of muscle, is ~88 kg. The computed BMI is ~33.5 (moderately obese). The subject has a heart pathology.

18.2.3 Respiratory Cycle and CAD Tissues Affected by Respiration Motion

The overall change in lung volume is set at 0.32 L, which is close to a normal-to-shallow breathing sequence for this subject. Default temporal resolution includes *12 discrete uniform steps* from 0 to 11 in steps of 1 from maximum exhalation to

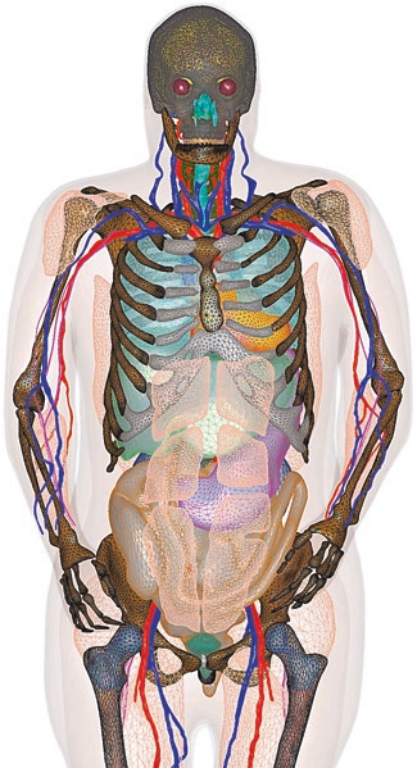

Fig. 18.4 Static VHP-Female v.3.1 CAD model at maximum exhalation (http://www.nevaem.com/)

maximum inhalation. The default full cycle includes *23 discrete steps*. Breathing cycles with finer resolution may be trivially constructed.

We choose the following major set of tissue parts (35 in total) to be affected by the respiratory motion:

- Lungs
- Ribcage with 24 ribs (every rib is moved *independently*)
- Thoracic cage cartilage
- Sternum
- Pectoralis muscles (major/minor)
- Abdominal muscles
- Erector spinae muscles
- Heart (muscle)
- Liver
- Stomach
- Outer shell – average body
- Outer shell – skin

These objects are transformed so that there are no intersections between any of them at any time moment, *with the minimum deformation factors*. These transformations are to be performed in global or local coordinate systems.

18.2.4 Required Accuracy: Total Body Mass

Since the respiratory motion modeled with multiple deformed CAD objects is an approximation, a requirement should be made with regard to the total mass error. We will require that the maximum relative body mass variation shall not exceed 0.1% during the entire respiratory cycle.

18.2.5 Algorithm

Below, we briefly review suggested kinematics and dynamics for the individual tissues. All quantitative approximations and the final formulas are thoroughly described in Appendix A.

Lung dynamics This is the first deformation step described in detail in Appendix A. In a local coordinate system associated with the top of the lung, the lung is deformed in all three directions and is moved in one direction in order to guarantee the expected diaphragm movement of 20 mm and simultaneously the volume change of 0.32 L, while maintaining anatomically sound overall deformations.

Thoracic cage kinematics This is the second deformation step. Since the rotation axes in Fig. 18.3 are very loosely defined for the actual anatomical data, we have rotated each rib pair about a fixed axis passing through the heads of two ribs (the end parts closest to the spine). We have also rotated slightly the rib pairs about the vertical axis. Thus, every rib pair is subject to rotation about two axes. All permissible variations of rotation angles have been tested, for every rib pair, in order to satisfy two criteria: (i) avoid intersections with the lung and (ii) stay as close to the lung as possible.

Sternum/cartilage dynamics This is the next deformation step. The sternum is subject to a translation motion, without rotation. Fixed *control points* on its surface are introduced. Those control points, along with the rib tips, form lines, along which the corresponding cartilage parts will further be deformed (moved and expanded).

Muscles dynamics In this case, we apply rotations, movements, and slight deformations. The goal is to minimize overall movement while avoiding intersections with the thoracic cage.

Heart kinematics The heart is moved in two respective directions without rotations and deformations. The cardiac cycle is not considered.

Liver/stomach kinematics Liver and stomach are moved in two respective directions and are slightly deformed; see Appendix A.

Outer full-body shells This is the only case where we cannot apply affine transformations. However, we may apply Boolean operations with the tissue CAD objects. A number of deformed chests objects are created internally, and then they are united with the otherwise static full-body shells. This operation requires greater care since we have two very closely spaced (1 mm) body shells.

18.2.6 Polynomial Interpolation

After a discrete set of affine transformations has been established, this set was converted to polynomials applicable to any temporal resolution and reported in Appendix A. The polynomial approximations have been independently tested with a fine grid. As an example, Table 18.2 reports affine polynomial approximations for several muscles. Note that the dynamic variable t in Table 18.1 is not the actual time, but is proportional to the diaphragm motion $x(t)$ in Eq. (18.1).

18.3 Results

The corresponding full-body VHP-Female model with the embedded respiratory motion in the form of a parametric sweep described in Appendix A has been independently realized in

- ANSYS Electronics Desktop software package
- CST Studio Suite software package
- MATLAB

The maximum body mass variation during the entire respiratory cycle is 80 g, *which is less than 0.1% of the total body mass*. The parametric sweep may be adjusted/modified at any time in response to further anatomical evaluations and customer needs.

18.3.1 RF Test at 300 MHz

The problem geometry is shown in Fig. 18.5. An incident plane wave at 300 MHz has a horizontal polarization. The simulations have been performed in ANSYS HFSS with three adaptive mesh refinement passes and with the final meshes approaching 1 M tetrahedra.

Near field Figure 18.5 shows the near-field results at three observation points given a 1 V/m incident wave. The scattered field is plotted. In the illuminated zone, the co-pol near field data may vary by about 3% due to the respiratory motion. In the

Table 18.2 Affine transformations of some muscles (inhalation only) of the VHP-Female model

		Muscles	Polynomials of deformation factors (angles recorded in degrees)
Pectoralis minor (in local CS)	*Left*	Rot z	$-7.149e-5*t^6+0.00252*t^5-0.03393*t^4+0.2181*t^3-0.681*t^2+1.406*t+0.005579$
		Move y	$0.0002042*t^6-0.007194*t^5+0.09695*t^4-0.6231*t^3+1.946*t^2-4.016*t-0.01594$
		Scale y	$2.042e-7*t^6-7.194e-6*t^5+9.695e-5*t^4-0.0006*t^3+0.001946*t^2-0.004*t+0.999984$
	Right	Rot z	$1.083e-05*t^6+8.348e-05*t^5-0.00957*t^4+0.1344*t^3-0.7021*t^2+1.774*t+0.01398$
		Move y	$-3.095e-5*t^6-0.0002385*t^5+0.02734*t^4-0.3841*t^3+2.006*t^2-5.067*t-0.03994$
		Scale y	$3.09e-8*t^6-2.385e-7*t^5+2.73e-5*t^4-0.00038*t^3+0.002*t^2-0.005067*t+0.99996$
Pectoralis major (in local CS)	*Left*	Move z	$-0.00013*t^6+0.004709*t^5-0.0656*t^4+0.4366*t^3-1.388*t^2+2.397*t-0.005142$
		Move y	$-0.05+0.0002525*t^6-0.00914*t^5+0.1272*t^4-0.8445*t^3+2.673*t^2-4.721*t+0.01132$
		Scale y	$2.6e-7*t^6-9.418e-6*t^5+0.0001312*t^4-0.00087*t^3+0.0028*t^2-0.0048*t+1.00001028$
	Right	Move z	$-4.642e-05*t^6+0.001553*t^5-0.02174*t^4+0.1655*t^3-0.6858*t^2+1.801*t+0.02082$
		Move y	$9.284e-05*t^6-0.003107*t^5+0.04348*t^4-0.331*t^3+1.372*t^2-3.602*t-0.04165$
		Scale y	$9.284e-8*t^6-3.107e-6*t^5+4.348e-5*t^4-0.00033*t^3+0.00137*t^2-0.0036*t+0.99995835$

(continued)

Table 18.2 (continued)

		Muscles	Polynomials of deformation factors (angles recorded in degrees)
Erector Spinae (in local CS)	*Left*	Scale y	$8.987e-06 * t^6 - 0.0003339 * t^5 + 0.004839 * t^4 - 0.03445 * t^3 + 0.1242 * t^2 - 0.2474 * t + 0.998756$
		Scale x	$4.493e-06 * t^6 - 0.0001669 * t^5 + 0.00242 * t^4 - 0.01723 * t^3 + 0.06208 * t^2 - 0.1237 * t + 0.9993778$
		Move y	$-1.123e-05 * t^6 - 0.0004174 * t^5 + 0.006049 * t^4 - 0.04307 * t^3 + 0.1552 * t^2 - 0.3093 * t - 0.3093$
	Right	Scale y	$-0.02 * t + 1$
		Scale x	$-0.02 * t + 1$
		Move y	$-0.05 * t$
Abdominal (in global CS)		Move z	$0.09091 * t * 10^{-3}$
		Move y	$-0.35 * t * 10^{-3}$

shadow zone, the corresponding variation is negligibly small. *Cross-polarization components may exhibit considerably larger relative near-field variations*.

RCS Figure 18.6 shows the monostatic radar cross section (RCS) of the heterogeneous breathing VHP-Female model during the respiratory cycle. The RCS variations are about 1%. More data may be acquired from the website www.nevaem.com.

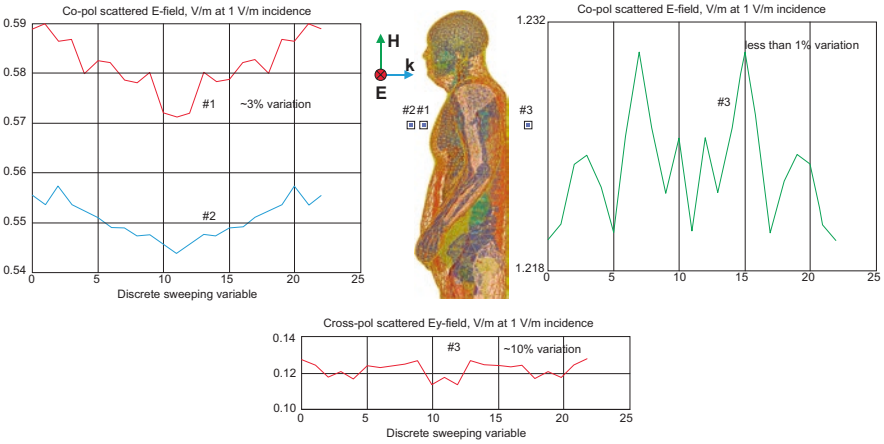

Fig. 18.5 Scattered field in the Fresnel region at 300 MHz

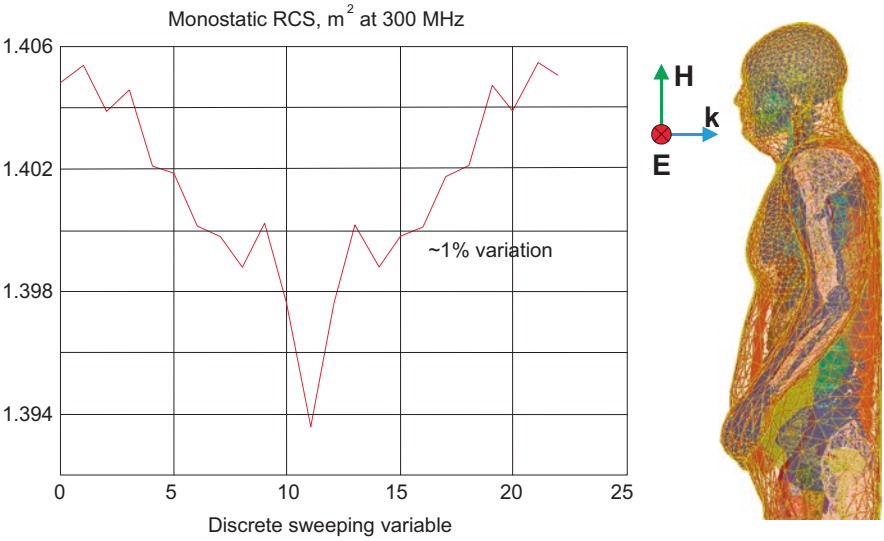

Fig. 18.6 Monostatic RCS during the respiratory cycle

Appendix A: Realization of the Respiratory Cycle for the VHP-Female CAD Model

Lung Deformation Sequence

New global coordinate system: Lung_CS. The origin is located at (0, max (Py), max (Pz)) with P being the point cloud of the lungs. The origin coordinates are given by

$$X = 0,\ Y = 122.8347,\ Z = -131.3727 \tag{18.A1}$$

Scaling in Lung_CS over N ($N = 11$) iterations total: Resulting Parametric Sweep in ANSYS

- 10% size increase in the z-direction: lung_scalez = $\left(1 + (0.1/N)\right)^{t}$
- 1% size increase in the x-direction: lung_scalex = $\left(1 + (0.01/N)\right)^{t}$
- 1% size increase in the y-direction: lung_scaley = $\left(1 + (0.01/N)\right)^{t}$

Variable t (sweeping variable, not time!) is running from 0 to N. This will result in the overall volume change from 2.22 L to 2.54 L, i.e., 0.32 L. Other sequences may be constructed in a similar fashion.

Translation in **Lung _ CS** over N ($N = 11$) iterations total: Resulting parametric sweep in ANSYS

- 3 mm overall in the y-direction: lung_movey = $-\frac{3}{\mathrm{N}} * t * 10^{-3}$ (m)

Rotation: None

Ribs Deformation Sequence

New global coordinate system: None

Scaling: None

Translation: None

Rotation: Every rib is rotated individually for a particular lung deformation so that there are no intersections between ribs and lungs given the minimum separation distance. Two rotation angles are used:

- Rotation about a rib axis, which is created by connecting two control points of two adjacent ribs closest to the vertebral column
- Rotation about the z-axis, in a new local CS, which is obtained by translation of the origin of the global CS to the rib control point(s) (individually for every rib)

Control points: Closest points to the vertebral column

Definition of rotation angles:

θ – Rotation angle about the rib axis, which results in an upward motion of the rib pair

φ – Rotation angle about the local z-axis, which results in an outward motion of the rib pair

See Tables 18.A1, 18.A2, and 18.A3

Sternum Deformation Sequence

New global coordinate system: **Sternum _ CS**. The origin is located at ((3∗(min (Px) + max (Px)/5), max (Py), (3∗max (Pz)/5)) with P being the point cloud of the sternum. The origin coordinates are given by

$$X = 20.78,\ Y = -28.86,\ Z = -290.3$$

Scaling: None

Translation: None

Rotation in **Sternum _ CS**: one degree about the new global y-axis over N ($N = 11$) iterations total.

Resulting parametric sweep in ANSYS

$$\text{sternum\_rot} = 0.09091 * \boldsymbol{t}.$$

Cartilage Deformation Sequence (Implemented in MATLAB)

New global coordinate system: None

Scaling: Two movement vectors are determined for every cartilage component at each iteration which will decide its scaling factor as follows:

$$New\ Movement\ Vector = \vec{m}_n$$

$$Old\ Movement\ Vector = \vec{m}_0$$

$$Scaling\ Factor = \left|m_n\right| \Big/ \left|m_0\right|$$

$$Scaling\ Vector = -m_n \Big/ \left|m_n\right|$$

Table 18.A1 Rib deformation sequence: table of computed control points (mm)

Coord./Rib Par#	1	2	3	4	5	6	7	8	9	10	11	12
X	44.690	43.810	43.42	44.11	39.57	32.07	30.61	34.9	34.31	35.91	46.5	54.13
	−27.49	−19.62	−17.15	−18.25	−13.45	−4.1	−1.296	−0.242	−1.062	−2.352	−10.33	−21.09
Y	58.37	80.38	91.95	104.3	107.7	104.5	106.3	103.3	102.7	106.3	112.5	109.3
	61.14	76.38	93.32	100.7	106.7	102.6	106.3	106.9	102.9	103	108	115.1
Z	−117.2	−131.4	−149.7	−167.3	−187.8	−215.3	−233.8	−260.5	−281.3	−306.4	−334	−367.3
	−121.7	−134	−156.6	−170	−192.2	−217.8	−232.7	−257	−279.9	−304.8	−334	−365.4

Table 18.A2 Rib deformation sequence: table of rotation angles (deg.) extracted from MATLAB

Iter. #/Rib pair #		1	2	3	4	5	6	7	8	9	10	11
$n_R = 1$	Θ	0.1667	0.3333	0.6667	0.8333	1.1667	1.5000	2.3333	3.0000	3.6667	4.3333	4.8333
	φ	0.0800	0.1600	0.3200	0.4000	0.5600	0.7200	1.1200	1.4400	1.7600	2.0800	2.3200
$n_R = 2$	Θ	0.6667	1.0000	1.3333	1.6667	2.0000	2.3333	2.6667	3.0000	3.3333	3.6667	4.0000
	φ	0.1600	0.2400	0.3200	0.4000	0.4800	0.5600	0.6400	0.7200	0.8000	0.8800	0.9600
$n_R = 3$	Θ	1.5000	2.0000	2.5000	3.0000	3.5000	4.0000	4.5000	5.0000	5.5000	6.0000	6.5000
	φ	0.2400	0.3200	0.4000	0.4800	0.5600	0.6400	0.7200	0.8000	0.8800	0.9600	1.0400
$n_R = 4$	Θ	0.6667	1.3333	2.0000	2.6667	3.3333	4.0000	4.6667	5.3333	6.0000	6.6667	7.3333
	φ	0.0800	0.1600	0.2400	0.3200	0.4000	0.4800	0.5600	0.6400	0.7200	0.8000	0.8800
$n_R = 5$	Θ	0.4167	0.6250	0.8333	1.0417	1.4583	1.8750	2.0833	2.5000	2.9167	3.1250	3.3333
	φ	0.8000	1.2000	1.6000	2.0000	2.8000	3.6000	4.0000	4.8000	5.6000	6.0000	6.4000
$n_R = 6$	Θ	0.2500	0.9583	1.6667	2.3750	3.0833	3.7917	4.5000	5.0000	5.2500	5.5000	5.7500
	φ	0.4000	1.5333	2.6667	3.8000	4.9333	6.0667	7.2000	8.0000	8.4000	8.8000	9.2000
$n_R = 7$	Θ	0.5833	0.8750	1.1667	1.4583	1.7500	2.0417	2.3333	2.6250	2.9167	3.2083	3.5000
	φ	0.8000	1.2000	1.6000	2.0000	2.4000	2.8000	3.2000	3.6000	4.0000	4.4000	4.8000
$n_R = 8$	Θ	0.6667	1.0000	1.3333	1.6667	2.0000	2.3333	2.6667	3.0000	3.3333	3.6667	4.0000
	φ	0.8000	1.2000	1.6000	2.0000	2.4000	2.8000	3.2000	3.6000	4.0000	4.4000	4.8000
$n_R = 9$	Θ	0.3750	0.7500	1.1250	1.5000	1.8750	2.2500	2.6250	3.0000	3.3750	3.7500	4.1250
	φ	0.4000	0.8000	1.2000	1.6000	2.0000	2.4000	2.8000	3.2000	3.6000	4.0000	4.4000
$n_R = 10$	Θ	0.4167	0.8333	1.2500	1.6667	2.0833	2.5000	2.9167	3.3333	3.7500	4.1667	4.5833
	φ	0.4000	0.8000	1.2000	1.6000	2.0000	2.4000	2.8000	3.2000	3.6000	4.0000	4.4000
$n_R = 11$	Θ	0.2292	0.4583	0.6875	0.9167	1.1458	1.3750	1.6042	1.8333	2.0625	3.6667	6.1875
	φ	0.2000	0.4000	0.6000	0.8000	1.0000	1.2000	1.4000	1.6000	1.8000	3.2000	5.4000
$n_R = 12$	Θ	0.5000	1.0000	1.5000	2.0000	2.5000	3.0000	3.5000	4.0000	4.5000	5.0000	5.5000
	φ	0.4000	0.8000	1.2000	1.6000	2.0000	2.4000	2.8000	3.2000	3.6000	4.0000	4.4000

Table 18.A3 Rib deformation sequence: table of rotation angles (deg.) extracted from MATLAB

Iter. #/Rib pair #		Polynomials of rotation angle (deg)
$n_R = 1$	Θ	$5.901e-05 * t^6 - 0.002019 * t^5 + 0.02502 * t^4 - 0.1346 * t^3 + 0.3259 * t^2 - 0.08703 * t + 0.006159$
	φ	$0.0001035 * t^6 - 0.00367 * t^5 + 0.0489 * t^4 - 0.3052 * t^3 + 0.9405 * t^2 - 1.114 * t + 0.5939$
$n_R = 2$	Θ	$0.3333 * t$
	φ	$0.08 * t$
$n_R = 3$	Θ	$0.5 * t$
	φ	$0.08 * t$
$n_R = 4$	Θ	$0.6667 * t$
	φ	$0.08 * t$
$n_R = 5$	Θ	$-1.844e-05 * t^6 + 0.0004494 * t^5 - 0.003782 * t^4 + 0.01514 * t^3 - 0.03083 * t^2 + 0.4792 * t - 0.001689$
	φ	$-3.54e-05 * t^6 + 0.0008629 * t^5 - 0.007261 * t^4 + 0.02908 * t^3 - 0.0592 * t^2 + 0.4488 * t - 0.003243$
$n_R = 6$	Θ	$0.45 * t$
	φ	$0.4 * t$
$n_R = 7$	Θ	$0.2917 * t$
	φ	$0.4 * t$
$n_R = 8$	Θ	$0.3333 * t$
	φ	$0.4 * t$
$n_R = 9$	Θ	$0.375 * t$
	φ	$0.4 * t$
$n_R = 10$	Θ	$0.4 * t$
	φ	$0.4167 * t$
$n_R = 11$	Θ	$2.986e-05 * t^6 - 0.00111 * t^5 + 0.01608 * t^4 - 0.1145 * t^3 + 0.4126 * t^2 - 0.09056 * t - 0.004135$
	φ	$2.156e-05 * t^6 - 0.000801 * t^5 + 0.01161 * t^4 - 0.08265 * t^3 + 0.2979 * t^2 + 0.01943 * t - 0.002985$
$n_R = 12$	Θ	$0.25 * t$
	φ	$0.5 * t$

Translation: A translation vector determines the movement of the cartilage for every iteration, given by:

$$Translation\ Vector = \vec{m}_n - \vec{m}_0$$

Rotation: The rotation axis and the rotation degree are given by:

$$Rotation\ Vector = \cos^{-1}\left(\vec{m}_n \cdot \vec{m}_0\right) / \left(\left|\vec{m}_n\right| \times \left|\vec{m}_0\right|\right)$$

$$Rotation\ Axis = \vec{m}_0 \times \vec{m}_n$$

See Tables 18.A4 and 18.A5

Muscle Deformation Sequence (Pectoralis Major, Pectoralis Minor, Abdominal Muscles, and Erector Spinae)

New local coordinate systems: A local coordinate system is defined for each muscle using a simple translation. The origins are located at (min(Px), max (Py), max (Pz)) with P being the point cloud of each left muscle and (max(Px), max (Py), max (Pz)) of each right muscle. Abdominal muscles are only transformed with respect to the global coordinate system: the origin at (0, 0, 0)

Scaling in local **CS**s: See the following tables for individual muscles

Translation in local **CSs**: See the following tables for individual muscles

Rotation in local **CS**s: See the following tables for individual muscles

See Tables 18.A6, 18.A7, 18.A8, 18.A9, 18.A10, 18.A11, 18.A12, 18.A13, and 18.A14

Heart Deformation Sequence

New local coordinate systems: According to literature, the pumping motion of the heart is independent of breathing. As a result, the heart object will only be transformed to avoid intersection with lungs in breathing sequence, with respect to the origin of the global coordinate system (0, 0, 0). See Tables 18.A15 and 18.A16

Table 18.A4 Cartilage deformation sequence: table of rotation angles (radians)

Iter. #/Cartilage pair #	1	2	3	4	5	6	7	8	9	10	11
Left1	0	0	0.01445	0.01388	0.01334	0.03706	0.03272	0.07020	0.01471	0.00713	0.00692
Right1	0	0	0.01445	0.01388	0.01334	0.03706	0.03272	0.07020	0.01471	0.00713	0.00692
Left2	0	0.02217	0.02194	0.02169	0.02143	0.02114	0.02084	0.02053	0.02021	0.01988	0.01954
Right2	0	0.02287	0.02281	0.02272	0.02260	0.02246	0.02230	0.02211	0.02190	0.02167	0.02142
Left3	0	0.03000	0.02975	0.02945	0.02910	0.02870	0.02826	0.02779	0.02728	0.02674	0.02618
Right3	0	0.02900	0.02858	0.02813	0.02763	0.02710	0.02655	0.02597	0.02537	0.02476	0.02413
Left4	0	0.03671	0.03598	0.03517	0.03430	0.03338	0.03242	0.03142	0.03041	0.02939	0.02837
Right4	0	0.03461	0.03470	0.03470	0.03461	0.03443	0.03416	0.03381	0.03338	0.03288	0.03231
Left5	0	0.01392	0.01361	0.01331	0.02113	0.02019	0.01195	0.01883	0.01801	0.01073	0.01049
Right5	0	0.01605	0.01575	0.01544	0.02521	0.02417	0.01399	0.02263	0.02167	0.01262	0.01234
Left6	0	0.00617	0.00610	0.00603	0.00596	0.00590	0.00583	0.00577	0.00571	0.00565	0.00559
Right6	0	0.01445	0.01388	0.01334	0.03706	0.03272	0.07020	0.01471	0.00713	0.00692	0.00672

Table 18.A5 Cartilage deformation sequence: table of expansion factors

Iter. #/Cartilage pair #	1	2	3	4	5	6	7	8	9	10	11
Left1	0	0.002864	0.004915	0.003289	0.005533	0.005889	0.013425	0.012064	0.012891	0.013652	0.011283
Right1	0	0.003292	0.005705	0.003689	0.006288	0.006622	0.015209	0.013425	0.014189	0.014884	0.012137
Left2	0	0.005041	0.005525	0.005993	0.006444	0.006876	0.007290	0.007685	0.008061	0.008417	0.008753
Right2	0	0.001314	0.001875	0.002430	0.002978	0.003518	0.004046	0.004562	0.005064	0.005552	0.006023
Left3	0	0.003696	0.004616	0.005512	0.006378	0.007211	0.008008	0.008765	0.009481	0.010153	0.010781
Right3	0	0.006657	0.007496	0.008297	0.009057	0.009774	0.010446	0.011073	0.011653	0.012188	0.012677
Left4	0	0.009183	0.010484	0.011701	0.012829	0.013864	0.014804	0.015651	0.016405	0.017069	0.017648
Right4	0	0.001770	0.000510	0.000766	0.002033	0.003287	0.004517	0.005714	0.006871	0.007980	0.009035
Left5	0	0.010654	0.010767	0.010868	0.023283	0.023299	0.011074	0.023284	0.023185	0.011103	0.011113
Right5	0	0.009079	0.009300	0.009506	0.020776	0.021132	0.010164	0.021585	0.021758	0.010557	0.010633
Left6	0	0.007867	0.007894	0.007918	0.007940	0.007959	0.007977	0.007992	0.008006	0.008017	0.008027
Right6	0	0.019481	0.019443	0.019386	0.062856	0.061347	0.165538	0.035730	0.016683	0.016521	0.016358

Table 18.A6 Origin coordinates for the local coordinate systems

Muscle	Local X (mm)	Local Y (mm)	Local Z (mm)	0.008753
Pectoralis minor left	89.03	27.64	−201.93	0.006023
Pectoralis minor right	−56.28	29.22	−189.24	0.010781
Pectoralis major left	18.83	76.19	−192.42	0.012677
Pectoralis major right	14.82	−31.92	−197.71	0.017648
Erector spinae left	0	146.73	−450.22	0.009035
Erector spinae right	0	146.79	−453.65	0.011113

Table 18.A7 Deformation factors for pectoralis minor left muscle. All angles are recorded in degrees

Configuration number	Rotation about Z axis (Θ)	Movement in Y direction	Scaling in Y direction
1	±0.9545	−2.7273	−0.0027
2	±1.2727	−3.6364	−0.0036
3	±1.9091	−5.4545	−0.0055
4	±2.2273	−6.3636	−0.0064
5	±2.8636	−8.1818	−0.0082
6	±3.1818	−9.0909	−0.0091
7	±3.8182	−10.9091	−0.0109
8	±4.1364	−11.8182	−0.0118
9	±4.4545	−12.7273	−0.0127
10	±5.0909	−14.5455	−0.0145
11	±5.4091	−15.4545	−0.0155

Table 18.A8 Deformation factors for pectoralis minor right muscle. All angles are recorded in degrees

Configuration number	Rotation about Z axis (Θ)	Movement in Y direction	Scaling in Y direction
1	± 1.2727	−3.6364	−0.0036
2	± 1.5909	−4.5455	−0.0045
3	±1.9091	−5.4545	−0.0055
4	±2.2273	−6.3636	−0.0064
5	± 2.5455	−7.2727	−0.0073
6	±3.1818	−9.0909	−0.0091
7	±3.8182	−10.9091	−0.0109
8	± 4.4545	−12.7273	−0.0127
9	± 5.0909	−14.5455	−0.0145
10	± 5.4091	−15.4545	−0.0155
11	± 6.0455	−17.2727	−0.0173

Table 18.A9 Deformation factors for pectoralis major left muscle. All angles are recorded in degrees

Configuration number	Movement in Z direction	Movement in Y direction	Scaling in Y direction
1	1.3636	−2.7273	−0.0027
2	1.8182	−3.6364	−0.0036
3	2.2727	−4.5455	−0.0045
4	2.7273	−5.4545	−0.0055
5	3.6364	−7.2727	−0.0073
6	4.0909	−8.1818	−0.0082
7	5.0000	−10.0000	−0.0100
8	5.4545	−10.9091	−0.0109
9	5.9091	−11.8182	−0.0118
10	6.3636	−12.7273	−0.0127
11	7.2727	−14.5455	−0.0145

Table 18.A10 Deformation factors for pectoralis major right muscle. All angles are recorded in degrees

Configuration number	Movement in Z direction	Movement in Y direction	Scaling in Y direction
1	1.3636	−2.7273	−0.0027
2	1.8182	−3.6364	−0.0036
3	2.2727	−4.5455	−0.0045
4	2.7273	−5.4545	−0.0055
5	3.1818	−6.3636	−0.0064
6	3.6364	−7.2727	−0.0073
7	4.0909	−8.1818	−0.0082
8	5.0000	−10.0000	−0.0100
9	5.4545	−10.9091	−0.0109
10	5.9091	−11.8182	−0.0118
11	6.8182	−13.6364	−0.0136

Table 18.A11 Deformation factors for erector spinea left muscles. All angles are recorded in degrees

Configuration number	Scaling in Y direction	Scaling in X direction	Movement in Y direction
1	−0.1600	−0.0800	0.2000
2	−0.2000	−0.1000	0.2500
3	−0.2400	−0.1200	0.3000
4	−0.2800	−0.1400	0.3500
5	−0.3200	−0.1600	0.4000
6	−0.3600	−0.1800	0.4500
7	−0.4000	−0.2000	0.5000
8	−0.4400	−0.2200	0.5500
9	−0.4800	−0.2400	0.6000
10	−0.5200	−0.2600	0.6500
11	−0.5600	−0.2800	0.7000

Table 18.A12 Deformation factors for erector spinea right muscles. All angles are recorded in degrees

Configuration number	Scaling in *Y* direction	Scaling in *X* direction	Movement in *Y* direction
1	−0.0200	−0.0200	0.0500
2	−0.0400	−0.0400	0.1000
3	−0.0600	−0.0600	0.1500
4	−0.0800	−0.0800	0.2000
5	−0.1000	−0.1000	0.2500
6	−0.1200	−0.1200	0.3000
7	−0.1400	−0.1400	0.3500
8	−0.1600	−0.1600	0.4000
9	−0.1800	−0.1800	0.4500
10	−0.2000	−0.2000	0.5000
11	−0.2200	−0.2200	0.5500

Table 18.A13 Deformation factors for abdominal muscles in the global coordinate system. All angles are recorded in degrees

Configuration number	Movement in *Z* direction	Movement in *Y* direction
1	−0.0909	−0.0909
2	−0.1818	−0.1818
3	−0.2727	−0.2727
4	−0.3636	−0.3636
5	−0.4545	−0.4545
6	−0.5455	−0.5454
7	−0.6364	−0.6363
8	−0.7273	−0.7272
9	−0.8182	−0.8181
10	−0.9091	−0.9090
11	−1.0000	−1.0000

Liver Deformation Sequence

New local coordinate systems: The liver object is deformed to avoid intersection with lungs in breathing sequence, with respect to the origin of a local coordinate system: (0, max (Py), max (Pz)). See Tables 18.A17, 18.A18, and 18.A19

Table 18.A14 Muscle deformations: Polynomials of deformation factors

		Muscles	Polynomials of deformation factors (angles recorded in degrees)
Pectoralis minor (in local CS)	*Left*	Rot z	$-7.149e-5*t^6+0.00252*t^5-0.03393*t^4+0.2181*t^3-0.681*t^2+1.406*t+0.005579$
		Move y	$0.0002042*t^6-0.007194*t^5+0.09695*t^4-0.6231*t^3+1.946*t^2-4.016*t-0.01594$
		Scale y	$2.042e-7*t^6-7.194e-6*t^5+9.695e-5*t^4-0.0006*t^3+0.001946*t^2-0.004*t+0.999984$
	Right	Rot z	$1.083e-05*t^6+8.348e-05*t^5-0.00957*t^4+0.1344*t^3-0.7021*t^2+1.774*t+0.01398$
		Move y	$-3.095e-5*t^6-0.0002385*t^5+0.02734*t^4-0.3841*t^3+2.006*t^2-5.067*t-0.03994$
		Scale y	$3.09e-8*t^6-2.385e-7*t^5+2.73e-5*t^4-0.00038*t^3+0.002*t^2-0.005067*t+0.99996$
Pectoralis major (in local CS)	*Left*	Move z	$-0.00013*t^6+0.004709*t^5-0.0656*t^4+0.4366*t^3-1.388*t^2+2.397*t-0.005142$
		Move y	$-0.05+0.0002525*t^6-0.00914*t^5+0.1272*t^4-0.8445*t^3+2.673*t^2-4.721*t+0.01132$
		Scale y	$2.6e-7*t^6-9.418e-6*t^5+0.0001312*t^4-0.00087*t^3+0.0028*t^2-0.0048*t+1.00001028$
	Right	Move z	$-4.642e-05*t^6+0.001553*t^5-0.02174*t^4+0.1655*t^3-0.6858*t^2+1.801*t+0.02082$
		Move y	$9.284e-05*t^6-0.003107*t^5+0.04348*t^4-0.331*t^3+1.372*t^2-3.602*t-0.04165$
		Scale y	$9.284e-8*t^6-3.107e-6*t^5+4.348e-5*t^4-0.00033*t^3+0.00137*t^2-0.0036*t+0.99995835$

(continued)

Table 18.A14 (continued)

		Muscles	Polynomials of deformation factors (angles recorded in degrees)
Erector spinae (in local CS)	*Left*	Scale y	$8.987e-06*t^6-0.0003339*t^5+0.004839*t^4-0.03445*t^3+0.1242*t^2-0.2474*t+0.998756$
		Scale x	$4.493e-06*t^6-0.0001669*t^5+0.00242*t^4-0.01723*t^3+0.06208*t^2-0.1237*t+0.9993778$
		Move y	$-1.123e-05*t^6-0.0004174*t^5+0.006049*t^4-0.04307*t^3+0.1552*t^2-0.3093*t-0.3093$
	Right	Scale y	$-0.02*t+1$
		Scale x	$-0.02*t+1$
		Move y	$-0.05*t$
Abdominal (in global CS)		Move z	$0.09091*t*10^{-3}$
		Move y	$-0.35*t*10^{-3}$

Table 18.A15 Deformation factors for the heart

Configuration number	Movement in Z direction	Movement in Y direction
1	−0.15	−0.05
2	−0.3	−0.1
3	−0.45	−0.15
4	−1.5	−0.5
5	−2.85	−0.95
6	−4.35	−1.45
7	−5.7	−1.9
8	−7.2	−2.4
9	−8.7	−2.9
10	−10.05	−3.35
11	−11.55	−3.85

Table 18.A16 Heart deformations: polynomials of deformation

Heart	Polynomials of deformation factors (angles recorded in degrees)
Move z	$-6.672\text{e}-06 * t^6 + 0.0008203 * t^5 - 0.02038 * t^4 + 0.2019 * t^3 - 0.917 * t^2 + 0.7346 * t - 0.03539$
Move y	$2.451\text{e}-06 * t^6 - 8.201\text{e}-05 * t^5 + 0.0009 * t^4 - 0.0015 * t^3 - 0.04611 * t^2 + 0.03447 * t - 0.0046$

Table 18.A17 Local coordinate system: liver

	Local X (mm)	Local Y (mm)	Local Z (mm)
Liver	0	120.136	−373.331

Table 18.A18 Deformation factors for the liver

Configuration number	Movement in Z direction	Movement in Y direction	Scale in Z direction
1	−0.18	−0.04	−0.001
2	−0.36	−0.8	−0.002
3	−1.44	−0.32	−0.008
4	−2.52	−0.56	−0.014
5	−3.6	−0.8	−0.020
6	−5.04	−1.12	−0.028
7	−6.48	−1.44	−0.036
8	−7.92	−1.76	−0.044
9	−9.36	−2.08	−0.052
10	−10.8	−2.4	−0.060
11	−12.24	−2.72	−0.068

Table 18.A19 Liver deformations: polynomials of deformation

Heart		Polynomials of deformation factors (angles recorded in degrees)
Move	*Z*	$-6.672e-06 * t^6 + 0.0008203 * t^5 - 0.02038 * t^4 + 0.2019 * t^3 - 0.917 * t^2 + 0.7346 * t - 0.03539$
Move	*Y*	$2.451e-06 * t^6 - 8.2e-05 * t^5 + 0.0009106 * t^4 - 0.001488 * t^3 - 0.0461 * t^2 + 0.0344 * t - 0.004638$
Scale	Z	$6.1e-8 * t^6 - 2.05e-6 * t^5 + 2.7e-5 * t^4 - 3.7e-5 * t^3 - 0.00115 * t^2 + 0.00086 * t + 0.99989$

Skin Shell Deformation

First, the skin shell deformation starts with a generation of N chest objects for each step via non-rigid transformations. This process was accomplished in MATLAB. A deformed chest region is defined as

$$141.3\,\text{mm} < P(:,1) < 173.4\,\text{mm}$$

$$P(:,2) < 64\,\text{mm}$$

$$-330.6\,\text{mm} < P(:,3) < -150.6\,\text{mm}$$

All nodes in the chest region of the skin shell are selected and transformed in the y-direction using the following equation:

$$P(:,2) = Pbase(:,2) - \frac{10}{N} * \boldsymbol{t} * \sin\left(P(:,3) - \min\left(P(:,3)\right)\right)$$

We chose nodes in the chest region so that $P(:,3) - \min(P(:,3))$ goes from 180 to 0. Therefore, nodes that are closer to the upper and lower boundaries of the region will move less than the nodes that are closer to the center. With maximum inhalation, the center node of the chest region will move by 10 mm in the Y direction. Thus, only coordinates of nodes belonging to the chest area are changed. Also, the connectivity matrix, t, of the entire skin shell still remains the same. As a result, 11 skin shell objects with different chest regions will be generated.

Second, these new skin shells are subtracted from the original skin shell in HFSS, which results in N smaller deformed chest objects. These chest objects are spaced evenly (400 mm in Y direction) in front of the original shell and then united. A moving box is carefully designed so that it covers only one chest object at any time instant *t*. Then, the intersection is performed. The process is illustrated in Fig. 18.A1.

Box original position is given by: $-300\text{mm}, (200 - \boldsymbol{t} * 400) * 10^{-3}, -350\text{mm}$.

An intersection operation is performed with the box and the chest array object, which results in one chest object for a particular time t. Finally, the chest object is moved and a unite operation is performed with the original skin shell (shown in Fig. 18.A2).

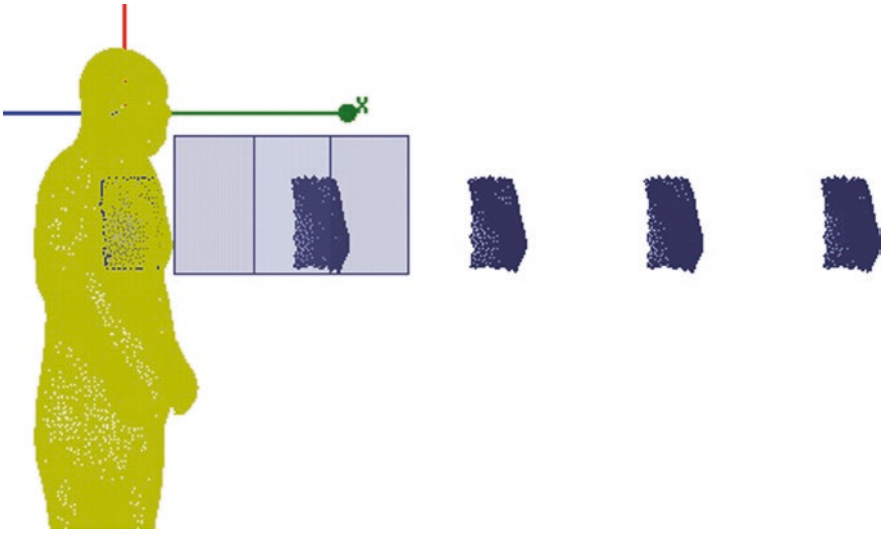

Fig. 18.A1 A box is carefully designed so that each iteration covers only one chest object at a time

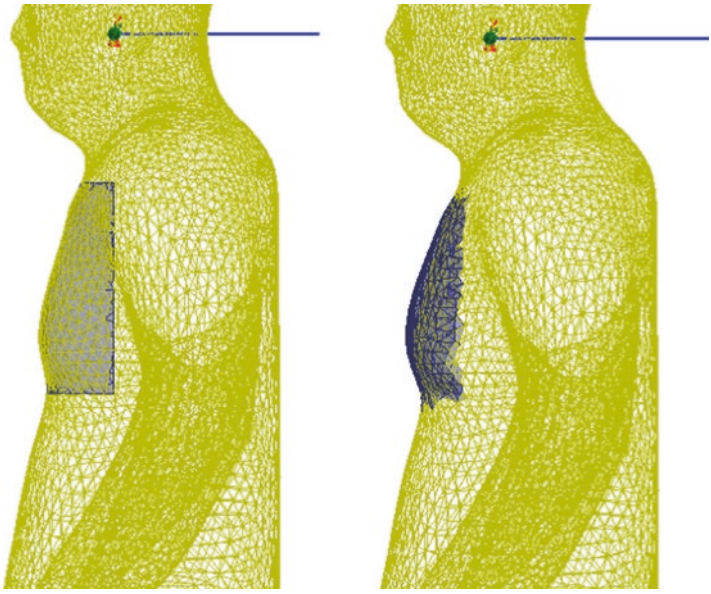

Fig. 18.A2 (**a**) (left). Skin Shell with $t = 0$. (**b**) (right). Skin shell with $t = 11$

References

1. Siebenthal, M. V. (2008). *Analysis and modelling of respiratory liver motion using 4DMRI*. Ph.D. dissertation, Elect. Eng. and Inform. Technology Dept., ETH Zurich, Switzerland.
2. Grimm, R., et al. (2015). Self-gated MRI motion modeling for respiratory motion compensation in integrated PET/MRI. *Medical Image Analysis, 19*, 110–120.
3. Lujan, A. E., et al. (1999). A method for incorporating organ motion due to breathing into 3D dose calculations. *Medical Physics, 26*(5), 715–720.
4. Lujan, A. E., Balter, J. M., & Ten Haken, R. K. (2003). A method for incorporating organ motion due to breathing into 3D dose calculations in the liver: Sensitivity to variations in motion. *Medical Physics, 30*(10), 2643–2649.
5. Segars, W. P., Lalush, D. S., & Tsui, B. M. W. (1999). Modelling respiration mechanics in the MCAT and spline-based MCAT phantom. *Nuclear Science Symposium*, Seattle, WA,, *2*, 985–989.
6. Wang, Y., Riederer, S., & Ehman, R. (1995). Respiratory motion of the heart: Kinematics and the implications for the spatial resolution in coronary imaging. *Magnetic Resonance in Medicine, 33*(5), 713–719.
7. West, J. (1995). *Respiratory physiology* (5th ed.). Baltimore: Williams and Wilkins.
8. Zeng, R.(2007). *Estimating respiratory motion from CT images via deformable models and priors*. Ph.D. dissertation, Elect. Eng. Dept., University of Michigan, Ann Arbor, Michigan.
9. Eom, J., et al. (2010). Predictive modeling of lung motion over the entire respiratory cycle using measured pressure-volume data, 4DCT images, and finite element analysis. *Medical Physics, 37*(8), 4389–4400.
10. Yanamadala, J., Noetscher, G. M., Louie, S., Prokop, A., Kozlov, M., Nazarian, A., & Makarov, S. N. (April, 2016). *Multi-purpose VHP-female version 3.0 cross-platform computational human model, 10th European conference on antennas and propagation 2016 (EuCAP16)*, Davos, Switzerland.
11. Hasgall, P. A., Di Gennaro, F., Baumgartner, C., et al. (13 Jan, 2015). *IT'IS database for thermal and electromagnetic parameters of biological tissues, version 2.6*.